Sensorless control of the charging process of a dynamic inductive power transfer system with interleaved nine-phase boost converter

Sensorless control of the charging process of a dynamic inductive power transfer system with interleaved nine-phase boost converter

Riccardo Ruffo, *IEEE student member*, Vincenzo Cirimele, *IEEE member*, Michela Diana, Mojtaba Khalilian, Alessandro La Ganga, and Paolo Guglielmi, *IEEE Member*

***Abstract*—The paper proposes a technique for the control of the charging process in a dynamic inductive power transfer system for automotive applications. This technique is based on an impedance control loop on the receiver side. The proposed control allows to carry out the different phases of the charging process in absence of a communication link between ground and vehicle side. The charging process starts with a sensorless procedure for the identification of the actual presence of the vehicle over the receiver. The same control technique introduces several advantages in terms of interoperability between systems having different requirements in terms of power demand. A $11\ \mathrm{kW}$ prototype has been implemented based on a transmitter 1.5 meters long as compromise solution between the long track coil and the lumped one. The power management of the receiver side is provided by a nine-phase interleaved boost converter. The experimental results prove the effectiveness of the proposed control together with a good matching with the developed theoretical equations set for the system description.**

***Index Terms*—Dynamic charging, electric vehicle (EV), inductive power transfer (IPT).**

I. Introduction

BATTERIES still represent the major obstacle to the diffusion of electric vehicles (EVs). Although the research in this field is leading to batteries with higher energy density, the typical range of EVs is still limited to few hundreds of kilometers. Hence, for long distance trips, the necessity of frequent and long stops for the recharge affects negatively the social perception about electric mobility. Inductive power transfer (IPT) is a promising technology able to increase the safety and the easiness of the charge. Moreover, its extension towards the so called dynamic IPT, allows the charge of the vehicle during the motion ideally eliminating the necessity of stops for the recharge.

In IPT systems for EVs, the transfer of electrical energy takes place by means of the magnetic coupling of a transmitter coil installed above or under the road surface and a receiver coil mounted under the vehicle floor. Different works in the last decades demonstrated the feasibility of IPT for applications aimed to the charge during the vehicle stops, called static IPT, with efficiency comparable to the classical plug-in systems [1]–[3]. Several static IPT systems will be available in the market in the next years. In fact, the standardization process has started and the release of the international standards SAE J2954 and the IEC 61980 related to static IPT for light EVs is planned within 2018 [4], [5].

Dynamic IPT introduces several issues due to the movement of the vehicle such as the necessity to rapidly identify the presence of the vehicle in order to energize the correct transmitter avoiding losses [6], the control of the transferred power in presence of unavoidable variations of the coupling between the coils [7], [8], the evaluation of the human exposure [9], [10]. These aspects are also related to the shape of the coils. In [11], [12] the adoption of a long transmitter having length of hundreds of meters is proposed. This shape allows a more continuous coupling that mirrors in a more continuous power transfer. According to the extension of the transmitter, the vehicle identification can be done with a slow dynamic [13]. Furthermore, each transmitter section can be powered by a single converter with advantages in terms of simplicity of the architecture and control of the system. However, a length of the transmitter much higher than the length of the receiver means a very low coupling between the coils that leads to the reduction of the efficiency and the presence of a strong stray field [6]. Other works propose the use of several consecutive small transmitters having comparable dimensions with respect to the receiver [14], [15]. In these applications, each transmitter is driven by a dedicated converter with increase in the system flexibility and tolerance to faults but with a collateral increase in the cost. The reduced dimension of the coils allows an increase of the magnetic coupling with consequent benefits in terms of efficiency and stray field reduction. However, for this kind of systems, the control is more difficult since the position of the vehicle must be detected very fast and the continuity of the power transfer is more difficult to be achieved [16]. In relation to these aspects, different power electronics (PE) architectures have been proposed together with some control techniques. Different papers as [2], [3], [17], propose the control of the power transfer from the only transmitter side while the receiver is connected to a passive diode rectifier. These methods enhance the simplicity of the control but limiting the regulation capability at the EV battery interface. Other works propose the use of active regulation

Manuscript received June 28, 2017; revised October 30, 2017; accepted January 21, 2018. This work was supported by European Union's 7th Framework Program for Research through the FABRIC project (No. FP7 605405) All authors are with the Department of Energy "Galileo Ferraris", Politecnico di Torino, Turin, Italy (e-mail: name.surname@polito.it).

also on the receiver side [18]–[21] but a large amount of them bases the effectiveness of the control on the presence of a communication link between the two sides [18]–[20]. These communication links are based on radio frequency technology [22] or on the use of additional coils or sensors [16]. The same solutions are adopted in [2], [18], [23] for the EV approaching identification. Nevertheless, all these methods become less robust for high vehicle speeds and all of them require the use of additional devices weakening the system fault-tolerance at the cost of increasing system cost and complexity.

This paper presents a completely sensorless control technique for dynamic IPT systems that allows to start, control and end the charge process by means of the only power electronics without any additional component or communication link between transmitter and receiver side. This technique is based on the control of the load impedance by means of a boost converter on the receiver side. This control allows the implementation of a simple technique for the identification of the presence of the vehicle above the transmitter together with the control of a continuous power transfer during the motion i.e. in presence of unpredictable variations of the magnetic coupling. At the same time, the proposed control technique offers the possibility to modify the power demanded by the vehicle without modifying the control operations on the transmitter side with considerable benefits in terms of interoperability and flexibility of the IPT system. These improvements represent a strong reduction of the system complexity and enhances the effectiveness of the control also for considerable vehicle speeds.

The developed IPT system and the basic equations set for its modeling are presented in Section II. Section III completes the description focusing on the PE's architecture adopted on the receiver side. The control technique in the different phases of the charging process is described in Section IV. In Section V are presented the experimental results carried out by the implementation of the control technique on a laboratory prototype for the testing in dynamic conditions.

II. System description

The general architecture of the developed prototype is shown in Fig. 1. The transmitter side is supplied by means of a SiC MOSFET based H-bridge that allows the creation of the high frequency field that links with the receiver coil. The receiver side is managed by a passive rectification stage and a DC/DC boost converter that interfaces with the battery. The coils, represented with the inductances L_1 and L_2, are compensated through the series connected capacitors C_1 and C_2. The magnetic coupling between the two coils is represented through their mutual inductance M. The coils resistances and the capacitors ESRs are modeled through the equivalent resistances R_1 and R_2. The series compensation has been chosen on both sides. With this compensation, the unavoidable variations of the coupling in dynamic applications do not cause significant variations in the resonant frequency of the system once the capacitors have been chosen [24]. With respect to higher order compensation topologies, the series-series compensation does not require additional elements (i.e. inductors)

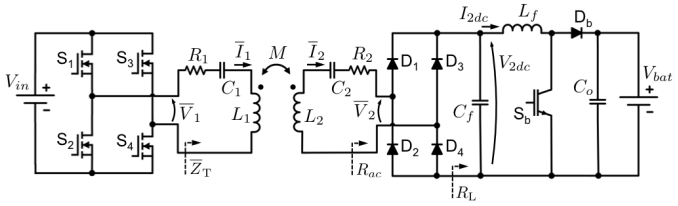

Fig. 1: Circuit diagram of the proposed IPT system.

for the compatibility of the commutations. With a view to repeat the proposed structure to create an IPT charging lane, this characteristic represents an important reduction on the overall infrastructure cost.

For the geometry of the coils, the developed system proposes the use of a compromise solution between the long track coil and the lumped one. This solution consists in the adoption of transmitters whose length is about half the length of a common passenger cars (about four meters) in order to guarantee that when a transmitter is activated, it is completely covered by the shape of the vehicle. This condition represents a strong increase in the safety of the application in relation to the electromagnetic field exposure [9]. Since the presented prototype is aimed to a widespread diffusion in the road infrastructures, the use of ferromagnetic materials has been limited uniquely to the receiver structure. This strongly reduces the cost per meter of the system together with the installation and maintenance costs. As secondary effect, the absence of ferromagnetic materials allows a lower value of self-inductance of the coil meaning a lower voltage stress over the reactive elements [25]. In these conditions, the values of self-inductance of transmitter and receiver are practically not affected by the relative position of the coils during the movement meaning a more precise and stable tuning of the resonance frequency.

The physical model of the system is based on the first harmonic approximation (FHA). This method is well-known in the domain of resonant converters and it allows to represent the system as working at a unique angular frequency ω_0 that is imposed by the source. ω_0 is the global resonant angular frequency of the system and it is put in relation with the reactive parameters of the IPT system by the relation:

$$\omega_0 = \frac{1}{\sqrt{L_1 C_1}} = \frac{1}{\sqrt{L_2 C_2}} \tag{1}$$

On the receiver side, the FHA allows to model the PE connected to the receiver with an equivalent resistor R_{ac} expressed as the ratio between the first harmonic of voltage and current at the input of the diode bridge:

$$R_{\mathrm{ac}} = \frac{V_2}{I_2} \tag{2}$$

For a series compensated receiver, R_{ac} can be expressed in terms of the quantities at the boost input as:

$$R_{\mathrm{ac}} = \frac{8}{\pi^2}\frac{V_{2dc}}{I_{2dc}} = \frac{8}{\pi^2} R_{\mathrm{L}} \tag{3}$$

The ratio between V_{2dc} and I_{2dc} is again a resistance here named *equivalent load resistance* R_{L}.

On the transmitter side, the voltage V_1 is controlled through a phase-shift modulation at fixed frequency. As illustrated in Fig. 2, this control is performed by modulating the phase angle α between the complementary square gate signal pairs according to the relation:

$$V_1 = \frac{2\sqrt{2}}{\pi} V_{in} \sin\left(\frac{\alpha}{2}\right) \tag{4}$$

A value of $\alpha = \pi$ rad leads to a pure square wave that corresponds to the maximum value of V_1.

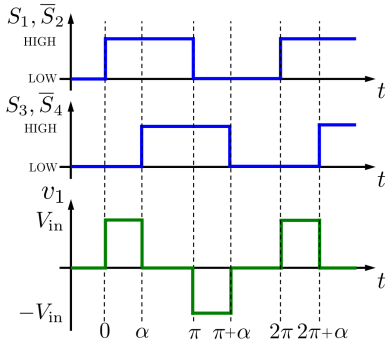

Fig. 2: Waveforms example of the phase-shift modulation. Gate signals of the H-bridge switches in blue. Related output voltage V_1 in green.

By writing the Kirchhoff's voltage law for the two sides of the IPT system, it is possible to describe it with the following equations set:

$$\begin{cases} \overline{V}_1 = R_1\overline{I}_1 + j\left(\omega L_1 - \dfrac{1}{\omega C_1}\right)\overline{I}_1 - j\omega M\overline{I}_2 & (5) \\ j\omega M\overline{I}_1 = R_2\overline{I}_2 + j\left(\omega L_2 - \dfrac{1}{\omega C_2}\right)\overline{I}_2 + R_{\mathrm{ac}}\overline{I}_2 & (6) \end{cases}$$

where $\overline{I}_1$ and $\overline{I}_2$ are the currents in the transmitter and in the receiver respectively. At the resonance ($\omega = \omega_0$) the terms in brackets become zero, $\overline{V}_1$ and $\overline{I}_1$ are in phase and their ratio results in an impedance having the only real component. This ratio is called *total impedance* $\overline{Z}_{\mathrm{T}}$ and expressed as:

$$\overline{Z}_{\mathrm{T}} = \frac{\overline{V}_1}{\overline{I}_1} = R_1 + \frac{\omega_0^2 M^2}{R_2 + R_{\mathrm{ac}}} \tag{7}$$

The currents on the two sides of the system can be expressed as:

$$\overline{I}_1 = \frac{R_2 + R_{\mathrm{ac}}}{R_1\left(R_2 + R_{\mathrm{ac}}\right) + \omega_0^2 M^2}\overline{V}_1 \tag{8}$$

$$\overline{I}_2 = \frac{j\omega_0 M}{R_1\left(R_2 + R_{\mathrm{ac}}\right) + \omega_0^2 M^2}\overline{V}_1 \tag{9}$$

Hence, the received power in the AC side results to be:

$$P_2 = R_{\mathrm{ac}}\left(\frac{\omega_0 M}{R_1\left(R_2 + R_{\mathrm{ac}}\right) + \omega_0^2 M^2} V_1\right)^2 \tag{10}$$

III. Interleaved Boost Converter

In the present work, the control of the load in the receiver side has been assigned to a unidirectional boost converter. This structure allows to regulate the input voltage in the range $0 - V_{\mathrm{bat}}$ for a power flow directed uniquely toward the battery. Despite this constraint, this structure has been preferred to a bidirectional boost as, for possible operations in discontinuous conduction mode (DCM), it presents negligible diode reverse recovery losses and lower turn-on losses of the switch [26].

The role of the boost converter is to control the voltage at the output of the diode rectifier in order to regulate the value of the resistance R_{ac} based on (3). As will be better detailed in Section V, the value of the load resistance is chosen in order to obtain the maximum power transfer in condition of nominal mutual coupling M_n. On the transmitter side, this condition coincides, by design, with the voltage V_1 at full square wave and the current I_1 at its nominal amplitude. This condition defines a nominal value of the total impedance $Z_{\mathrm{T,n}}$:

$$Z_{\mathrm{T,n}} = \frac{V_1\,|_{\alpha=\pi}}{I_1} = R_1 + \frac{\omega_0^2 M_n^2}{R_2 + R_{\mathrm{ac}}} \tag{11}$$

Hence, the reference value of resistance that has to be controlled by the boost converter can be expressed as:

$$R_{\mathrm{L}}^* = \frac{\pi^2}{8} R_{\mathrm{ac}}^* = \frac{\pi^2}{8}\left(\frac{\omega_0^2 M_{\mathrm{n}}^2}{Z_{\mathrm{T,n}} - R_1} - R_2\right) \tag{12}$$

The necessity of emulation of a resistive load with a fast transient response, with respect to the transmitter side control, has led to the choice of an interleaved architecture for the boost converter. As shown in Fig. 3, the implemented converter consists of a nine-phase interleaved boost converter where each leg is based on an IGBT. Each leg operates with a phase shift of $40°$. In this way, the ripple currents in the inductors $L_{f1}, ..., L_{f9}$ tend to cancel each other reducing the ripple in the input current I_{2dc}. Moreover, the frequency of the ripple is moved at nine times the PWM period. Equation (13) expresses the peak-to-peak ripple of the current at the boost converter input ΔI_{2dc} normalised with respect to the maximum value of

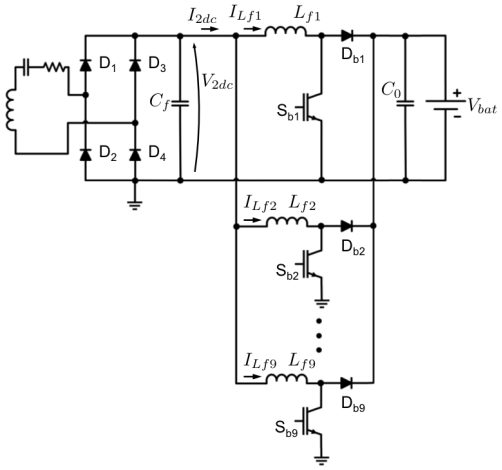

Fig. 3: Circuit diagram of the interleaved 9-phase boost converter on the receiver side.

the ripple for a classical 1-phase boost converter $\Delta I_{2dc,\max}$. This worst case condition occurs for a duty cycle $D = 0.5$.

$$\frac{\Delta I_{2dc}}{\Delta I_{2dc,\max}} = 4\frac{(N\cdot D-[N\cdot D])\,(1-(N\cdot D-[N\cdot D]))}{N} \quad (13)$$

Equation (13) refers to the continuous conduction mode (CCM) and it is generalized for N interleaved phases where the square bracket notation is used to indicate the integer part. The resulting behavior of the ripple is shown in Fig. 4 for different number of interleaved phases and values of the duty cycle. It can be seen from Fig. 4 that the current ripple

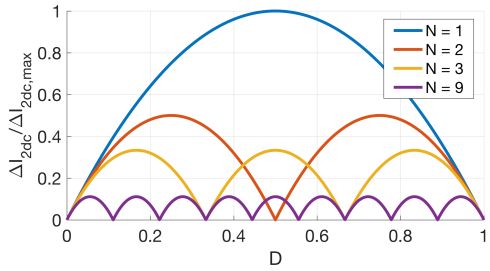

Fig. 4: Peak-to-peak ripple of the boost converter input current I_{2dc} for different interleaved phases normalized with respect to the ripple in the worst-case ($N=1$, $D=0.5$).

at the input of the nine-phase converter is strongly reduced with respect to the single boost converter. The effect of the interleaving reflects also on the reduction of the rms current in the capacitors C_f and C_0. This improves the effectiveness of these filters whom dimensions can be strongly reduced [27]. In order to simplify as much as possible the converter circuitry, the unit of the developed converter is constituted of a 3-phase Intelligent Power Module (IPM). As each IPM is designed to operate at a maximum switching frequency around 20 kHz, the use of three modules naturally allows to operate with a ripple frequency compatible with the frequency of the ripple at the diode bridge output (i.e. 170 kHz).

IV. Equivalent Load Control Operations

A. Power control in dynamic conditions

As introduced in the previous sections, the main principle of the proposed control technique consists in keeping the value of the equivalent load impedance constant through the active regulation provided by the boost converter. This technique allows to regulate the power transfer in presence of variations of the mutual coupling by acting on the only transmitter side that means to regulate the only voltage V_1 by varying the angle α. This regulation can take place without any information exchange between the vehicle and the ground.

The block scheme of the H-bridge control is shown in Fig. 5. It basically consists of a PI controller whose output is the angle α (saturated between 0 and 180°). The control directly operates on the peak of the transmitter current I_1. This current is measured through a high-frequency current transformer (HFCT). Hence, the output current of the HFCT is rectified and multiplied by a scaling factor $2\sqrt{2}/\pi$ and the transformer ratio t. The obtained value is a reconstruction of the transmitter current peak $\hat{I}_1$ that can be compared with the

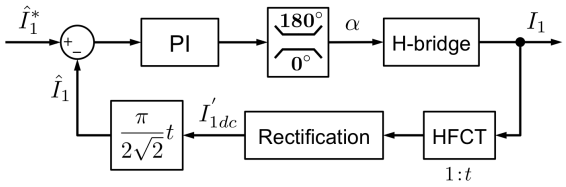

Fig. 5: Control block scheme of the H-bridge.

reference current peak $\hat{I}_1^*$. The reference value is set to the rated value of the current that is the same value used in (11). According to (8) and (9), if the value of mutual inductance decreases due to the misalignment between transmitter and receiver, both currents tend to increase. In that case the control in the transmitter reacts limiting the current I_1 by reducing the rms value of V_1.

If the mutual inductance becomes higher than the nominal value $M_{\rm n}$, the control tries to force the rated value of the current by saturating the voltage V_1 whose waveform remains a pure square wave as in the nominal condition. In this circumstance, the currents and the power are intrinsically limited by the systems i.e. the total impedance $Z_{\rm T}$. This condition can be due, for example, to a too heavy load, tires not perfectly inflated or simply for reasons of interoperability among vehicles having different heights.

In the present work, the H-bridge operates at fixed frequency equal to 85 kHz in compliance with the standard SAE J2954 [5] as a base for future interoperability between static and dynamic systems.

B. Interleaved boost converter control

The control block diagram of the nine-phase boost converter is shown in Fig. 6. It is composed by a single outer loop which deals with the impedance control and nine inner loops which are responsible for the current control of each phase. The input reference of the outer loop is the equivalent load resistance $R_{\rm L}^*$ which value is multiplied by the measured current I_{2dc} at the input of the converter. In this way the impedance control becomes a classical voltage control that regulates the voltage V_{2dc}. The global reference current I_{2dc}^* is obtained at the output of the PI controller. This reference value is divided by nine in order to have the reference current for each of the nine different inner loops. The reference current is saturated between $I_{\min}$ and $I_{\max}$. The value of $I_{\max}$ is equal to the maximum current that the single phase can drain. The value of $I_{\min}$ is chosen slightly higher than zero in order to maintain the short-circuit condition during the identification and start-up phase by saturating the PI controller of the current loop. The motivations at the base of this choice are clarified in the next sections.

In each inner loop, the reference current is compared with the measured value of the current in the respective phase. The resulting error is filtered by a PI controller and normalized with respect to the actual value of the battery voltage $V_{\rm bat}$. This normalization allows to maintain the control loop bandwidth independent of the variation of $V_{\rm bat}$. The resulting signal is compared with a triangular carrier obtaining the gate signals

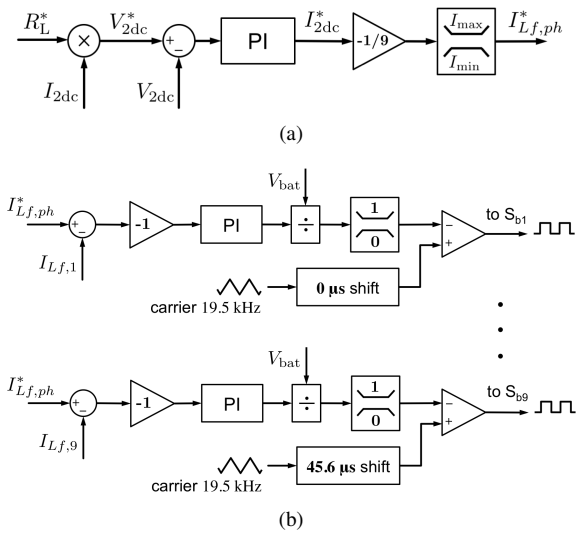

Fig. 6: Control block scheme of the DC/DC boost converter. (a) Outer impedance loop. (b) Inner nine-phase current-sharing loop.

for each phase switch. The gate signals have the same fixed frequency of 19.5 kHz and the same duty cycle but each leg operates with a phase shift of $2\pi/9$ rad. The role of the saturation block is to limit the modulating signal between 0 and 1 in relation to the triangular carrier that has the same amplitude. The gain blocks having negative sign are used in accordance with the adopted convention for the currents depicted in Fig. 3.

C. Self vehicle presence identification and start-up

The active regulation of the equivalent load introduces the possibility to develop a procedure for the sensorless and automatic identification of the vehicle. This procedure, mandatory for the improvement of the safety and the effectiveness of the overall charging process, completes the sequence of tasks necessary to carry out the cycle of power transfer in dynamic conditions.

Differently from previous works that propose the use of additional coils or sensors for the detection [2], [16], [17], the technique here proposed is based on the only power electronics control without requiring any additional sensing. This technique is based on the monitoring of the angle α when the H-bridge controls a certain reference current $\hat{I}_1^*$ whose value is much lower than the nominal reference value. If the vehicle is absent, the only parameter that limits the current is the coil resistance R_1. Hence, the value of α is very small according to the extremely low voltage required to force the flowing of the transmitter current. When a vehicle approaches the transmitter, the mutual coupling with the receiver starts to increase together with the value of the total impedance. In this condition, the value of α can be expressed as:

$$\alpha = 2\sin^{-1}\left(\frac{\pi \hat{I}_1^* Z_{\mathrm{T}}}{2\sqrt{2}V_{\mathrm{in}}}\right) \tag{14}$$

The increase of Z_{T} causes a decrease in the actual current I_1. To react against this decrease, the converter has to increase the value of the voltage by increasing the value of the angle α. At the moment that α reaches a certain threshold value α_{on}, the vehicle presence is considered verified and the transmitter can be energized at the rated current.

The same technique is used to turn-off the converter when the vehicle leaves the transmitter or if the misalignment becomes too high to guarantee the effectiveness of the commutations of the H-bridge switches. If α falls below a certain threshold α_{off} the system is turned off.

During the phase of approach to the charging lane, the receiver is maintained short-circuited by the boost converter ($R_{\mathrm{L}}^* = 0$). In this way, when the coupling becomes significant, the value of the total impedance is the highest possible. This forces α to reach the threshold value in the most rapid way. When the threshold is reached, $\hat{I}_1^*$ is switched from the value for the identification to the nominal value via a ramp variation.

On the receiver side, the current loop of the boost converter provides a reference current $I_{Lf,ph}^* = I_{\min}$. As the value of $I_{\min}$ is not zero, the impedance loop controls the short-circuit of the receiver but the PI controller starts to accumulate error as I_{2dc} is equal to zero according to the absence of induced voltage. Once the vehicle approaches the transmitter during the identification phase, the coupling becomes higher than zero and the current I_{2dc} starts to increase. The short circuit is maintained as long as the error accumulated in the PI becomes zero. When this condition occurs, the control starts to control the desired value of equivalent load by releasing the short-circuit. This instant marks the beginning of the charging process. It is worth mentioning that, the PI error is saturated through an anti-wind up in order to avoid that the short-circuit condition is maintained for too long.

The efficiency of the identification process can be increased by energizing the transmitter only for 1 ms over a period of 2 ms. This allows to maintain a practically full exploitation of the transmitter length for reasonable speed of the vehicle while strongly reducing the losses. At a vehicle speed of 100 km/h, this proposed technique can guarantee the vehicle identification with the same performance of a continuous energization.

As done for the identification phase, the charge process is automatically ended once the value of α becomes equal or lower than a certain angle α_{off} by turning the H-bridge off. After this event, the control returns to the identification state in order to be ready in case of approach of a new vehicle.

D. Power demand regulation

Another important aspect of the equivalent load control consists in the possibility to regulate the amount of received power P_2 by simply modifying the value of R_{L}^*. This can be deduced from (8), (10) and (12). As indicated by (7), modifications of the equivalent load mirror in a variation of the total impedance. This variation can be managed by the H-bridge control without requiring any modification in the control parameters. This means that also this kind of regulation can be carried out without the necessity of any information exchange between the two sides of the IPT system.

This aspect represents another important benefit in terms of interoperability as any kind of vehicle in any battery state of charge can decide its own level of received power while the control of the transmitter remains unvaried.

In a real implementation, this characteristic is fundamental to make the IPT system able to supply vehicles that, for reasons of weight, maximum speed etc. need for a power lower than the rated power of the system. The same regulation capability can be applied is conditions of traffic jam. In this case, the vehicle is stopped so it does not need to receive the rated power but only the limited amount necessary to supply the ancillary services as on-board electronics or air-conditioning. In this case, the value of R_{L}^{*} can be set in order to receive this limited amount of power while the transmitter side operations remain unvaried.

V. Experimental validation

A. Experimental setup

The proposed control of the charging process has been implemented on the laboratory prototype depicted in Fig. 7. The prototype is based on a transmitter coil having inner dimensions 1.5 m in length and 0.5 m in width and a receiver coil of 0.3 m in length and 0.55 m in width hosted in a dedicated magnetic structure further detailed in [28]. The receiver structure has been mounted on a movable metallic carriage that emulates the vehicle. The lateral misalignment and the height of the receiver structure can be regulated by means of two different mechanisms controlled through two stepper motors. This arrangement assures the possibility to test the system in dynamic conditions under different possible conditions of misalignment. The entire system is powered though a 3-phase insulation transformer rectified by means of a diode bridge. A 50 kW battery emulator is connected to the boost converter in order to emulate the vehicle battery. This systems allows a high flexibility in the prototype testing offering the possibility to operate without necessity of power dissipation. The H-bridge control is implemented with an MC56F84550 DSC while the boost converter is controlled though an XC3S200A FPGA. Two 8 bit digital oscilloscopes at the sampling rate of 5 MS/s are used to register the waveform on the two sides of the system. Both oscilloscope acquisitions have been triggered on the voltage V_{2dc}.

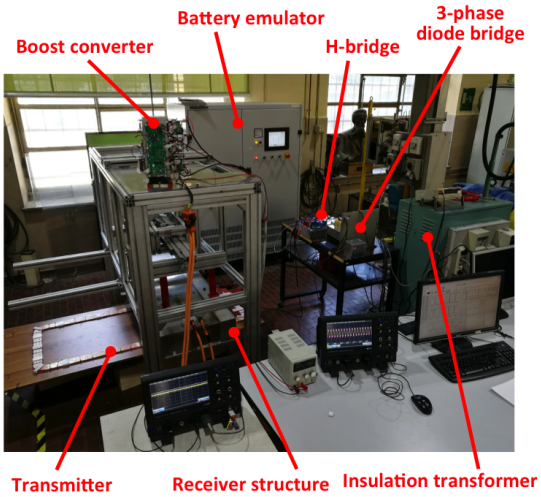

Fig. 7: Experimental prototype and test setup.

The system parameters are reported in Table I. In nominal conditions, i.e. nominal electrical parameters, nominal distance and perfect alignment of the coils, the system is capable to transfer 11 kW to the battery by controlling a nominal current peak $\hat{I}_1 = 40.3$ A. According to (12), the reference value for the impedance-matching loop has been set to $R_{\mathrm{L}}^{*} = 4.2\ \Omega$.

TABLE I: IPT system specifications and parameters

Parameters	Symbol	Value
Nominal power	P_{bat}	11 kW
Working frequency	f_0	85 kHz
DC input voltage	V_{in}	500 V
Nominal transmitter current	I_1	28.5 A
Nominal total impedance	$Z_{\mathrm{T,n}}$	15.8 Ω
Nominal receiver current	I_2	50 A
Nominal battery voltage	V_{bat}	370 V
Transmitter self-inductance	L_1	281.4 μH
Receiver self-inductance	L_2	119.8 μH
Nominal mutual inductance	M_{n}	14.3 μH
Transmitter resistance	R_1	0.78 Ω
Receiver resistance	R_2	0.53 Ω
Transmitter capacitor	C_1	12.5 nF
Receiver capacitor	C_2	29.2 nF

The results of three different tests are here presented. The first one aims to demonstrate the control effectiveness in presence of variations of the mutual coupling in static and dynamic conditions. The second one focuses on the identification of the vehicle presence above the transmitter coil and the automatic starting and ending of the charging process. The last test proves the possibility to regulate the demanded power acting on the only receiver side by modifying the equivalent reference load resistance.

B. Control at variable coupling

The effectiveness of the control has been checked in static conditions for different values of the mutual inductance M by varying the lateral misalignment and the distance of the receiver. The experimental results have been compared with the theoretical behavior based on the model and equations previously presented. The measurements have shown a general good matching with the model as shown in Fig. 8. The value of the H-bridge output voltage V_1 has been evaluated by applying a fast Fourier transform to the measured waveform. This spectral analysis has allowed to isolate the only fundamental component at 85 kHz used for the first harmonic approximation. Differently, the oscilloscope does not provide the same results as it returns the true rms of the waveform by taking into account the overall harmonic content. For the sake of completeness, a comparison between the two approaches is provided in Fig. 8a.

Fig. 8e shows that the rated power is transferred only in correspondence of the nominal coupling i.e. $M = M_{\mathrm{n}}$. In presence of misalignment ($M < M_{\mathrm{n}}$) the current I_1 is limited by the H-bridge control that decreases the voltage V_1. The reduction of coupling consequently reduces the receiver current reducing

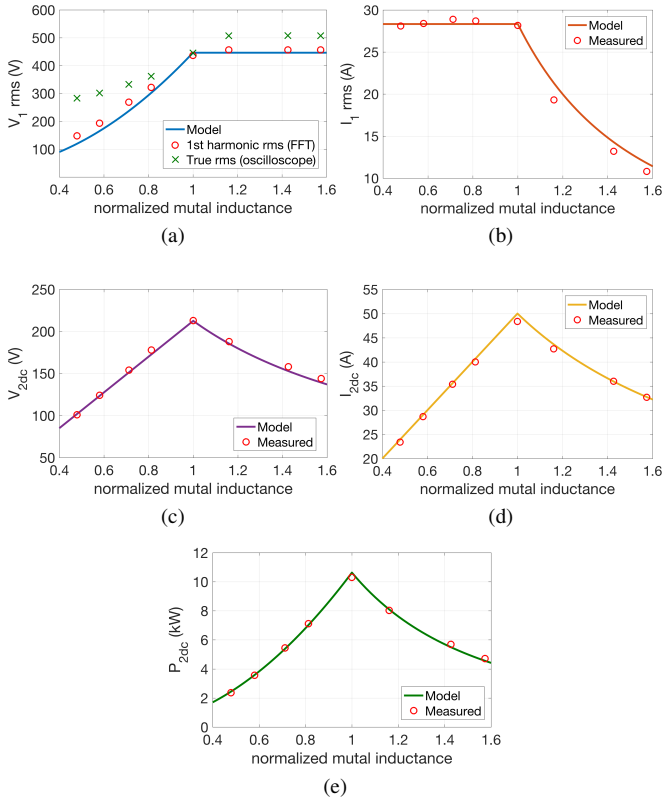

Fig. 8: Theoretical and measured behavior of voltages and currents of the IPT system controlled through the impedance control technique under dynamic/variable coupling conditions. The values of mutual inductance are normalized with respect to the nominal value $M_{\rm n} = 14.3$ μH. (a) Transmitter rms voltage V_1. (b) Transmitter rms current I_1. (c) Boost converter input voltage V_{2dc}. (d) Boost converter input current I_{2dc}. (e) Power at the boost converter input.

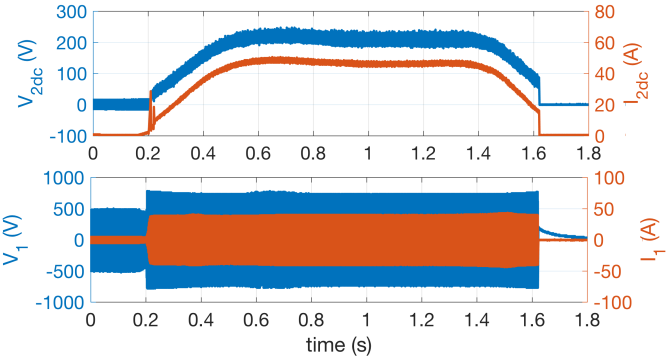

Fig. 9: Representative waveforms during the passage of the vehicle over one transmitter.

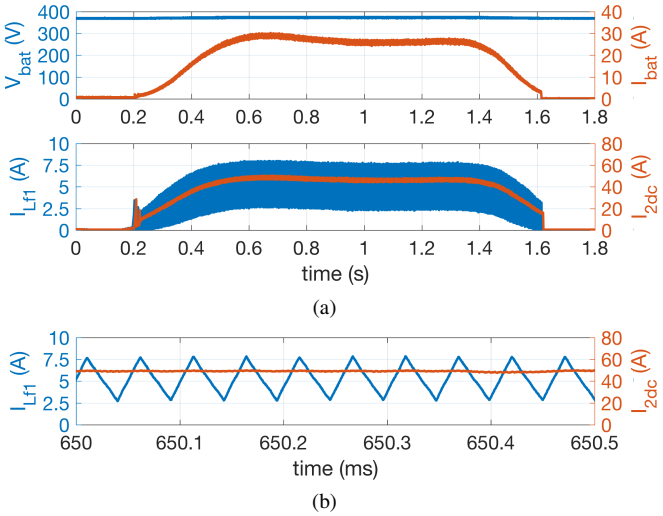

Fig. 10: Detail of the effect of the interleaving over the current ripples. (a) Waveforms on battery side and boost converter for a complete passage of the vehicle. (b) Zoom over one phase ripple.

the amount of transferred power. If the receiver gets closer to the transmitter ($M > M_{\rm n}$), the H-bridge tries to force the nominal current by saturating V_1 to its maximum value which corresponds to a pure square waveform. The H-bridge is no more able to control the current I_1 but its value is intrinsically kept limited by the effect of the coupling or, in other words, by the increased value of the total impedance $Z_{\rm T}$.

In a second step, the control has been tested in dynamic conditions in absence of lateral misalignment at a speed of about 4 km/h. The result is shown in Fig. 9. After the vehicle identification, the charge process starts letting the power transfer led by the variation of coupling. When the receiver is entirely above the transmitter, the transferred power remains practically constant at the rated level. The effect of the interleaving on the reduction of the current ripple is shown in Fig. 10.

The same test has been repeated by setting a gradual lateral misalignment during the movement. This case emulated a more realistic working condition of the IPT system where the alignment is not kept fixed by mechanical alignment or autonomous driving systems. Also in this case the control has been proven to be effective and robust as shown in Fig. 11. By comparing Fig. 9 and Fig. 11, one can note that the functioning of the transmitter side remains unvaried for both tests while the transferred power profile follows the coupling variations in a continuous and stable way. The system automatically turns off when the mutual inductance becomes lower than about 5 μH, that corresponds to a lateral misalignment of about 30 cm, or a complete exit of the receiver above the transmitter. This condition corresponds to a turn off angle $\alpha_{\rm off} = 40°$.

C. Identification procedure

For the identification procedure, the proper values of the angle $\alpha_{\rm on}$ and the reference current $\hat{I}_1^*$ have been empirically identified. Laboratory trials have aimed to search the minimum values of $\alpha_{\rm on}$ and $\hat{I}_1^*$ assuring a robust and fast vehicle presence identification. The tests have led to the selection of a threshold angle $\alpha_{\rm on} = 7°$ in correspondence to a reference current $\hat{I}_1^* = 2\sqrt{2}$ A. As introduced in Section IV-C, this angle has been identified for a short-circuited receiver. As shown in Fig. 12, this condition forces the value of the total impedance

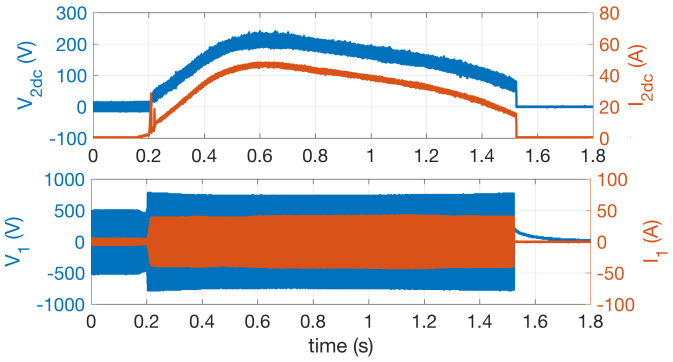

Fig. 11: Representative waveforms during the passage of the vehicle over one transmitter with gradual lateral misalignment of the vehicle.

to its maximum value forcing in this way a faster transition of the angle α towards the activation threshold. This condition cannot be otherwise reached for the nominal reference value of R_{L} especially in presence of strong initial misalignment of the vehicle.

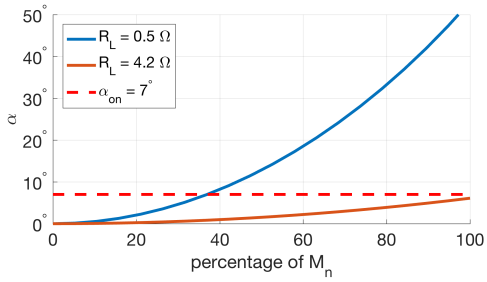

Fig. 12: Variation of the angle α with respect to different values of the mutual inductance represented as percentages of the rated value $M_{\mathrm{n}} = 14.3\ \mu\mathrm{H}$. The two behaviors are shown for two different values of the equivalent load resistance and for the same value of the reference current $\hat{I}_1^* = 2\sqrt{2}$ A.

Several tests have been performed in order to find the limits of the identification procedure. The chosen parameters have allowed to correctly recognize the presence of the vehicle up to an initial misalignment of 30 cm. This misalignment has been proven to be the limit of regulation capability of the control in correspondence of which the system automatically turns off.

When the vehicle reaches the transmitter, the effect of the coupling forces the current to a lower value. Hence, the H-bridge reacts by increasing the angle α. Once the turn on threshold is reached, the reference current becomes equal to the nominal value of 28.5 A via a ramp variation and the transmitter is fully energized. The turn-on threshold is reached when the shape of the receiver coil starts to overlap the transmitter. This condition corresponds to a value of the mutual inductance of about 40% of the nominal value.

In correspondence to the coupling increase, the induced current that starts to flow in the receiver decreases the accumulated error in the PI controller of the current-sharing loop. When the PI integral term is cancelled, the impedance control starts to regulate the desired equivalent load. The boost switches start to commutate allowing the charge of the capacitor C_f and the power transfer.

D. Power demand regulation

Finally, the behavior of the control for different values of R_{L}^* has been tested. Fig. 13 shows the theoretical and experimental behavior of the control tested at the nominal coupling. Also in this case, the experiments demonstrated a good matching with the model and the capability of the system to regulate the power by varying the only equivalent load at the receiver side. As shown in Fig. 13c, the power can be regulated by both increasing or decreasing R_{L} with respect to the nominal value. However, the regulation behavior is not independent of the direction of this variation. If the power is controlled by decreasing the value of R_{L}, the output power changes linearly with the resistance. For an increase of R_{L}, the power varies with a hyperbolic relationship. Moreover, this variation has not the same effect on the efficiency. Fig. 13d shows the effect on the efficiency measured between the H-bridge output and the interleaved boost converter input. Values of R_{L} lower than the nominal one cause a strong limitation in the transferred power causing a decrease in the efficiency and increasing the power dissipation into the receiver. In contrast, an increase of R_{L} leads to a reduction of the transferred power but maintaining a high efficiency of the system. This variation has

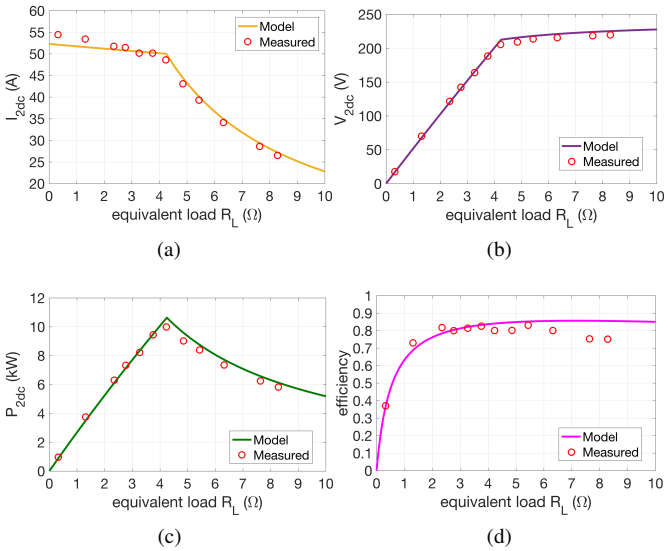

Fig. 13: Theoretical and measured behaviour of receiver quantities of the IPT system in presence of variations of the controlled equivalent load. (a) Boost converter input current I_{2dc}. (b) Boost converter input voltage V_{2dc}. (c) Received power P_{2dc}. (d) Efficiency from H-bridge output to boost input.

an opposite effect on the H-bridge commutations efficiency. In fact, as visible in Fig. 14, when the equivalent resistance increases, the transmitter current remains at its nominal value but the transmitter voltage cannot remain a square wave. Conversely, when R_{L} is lower than the nominal value, the

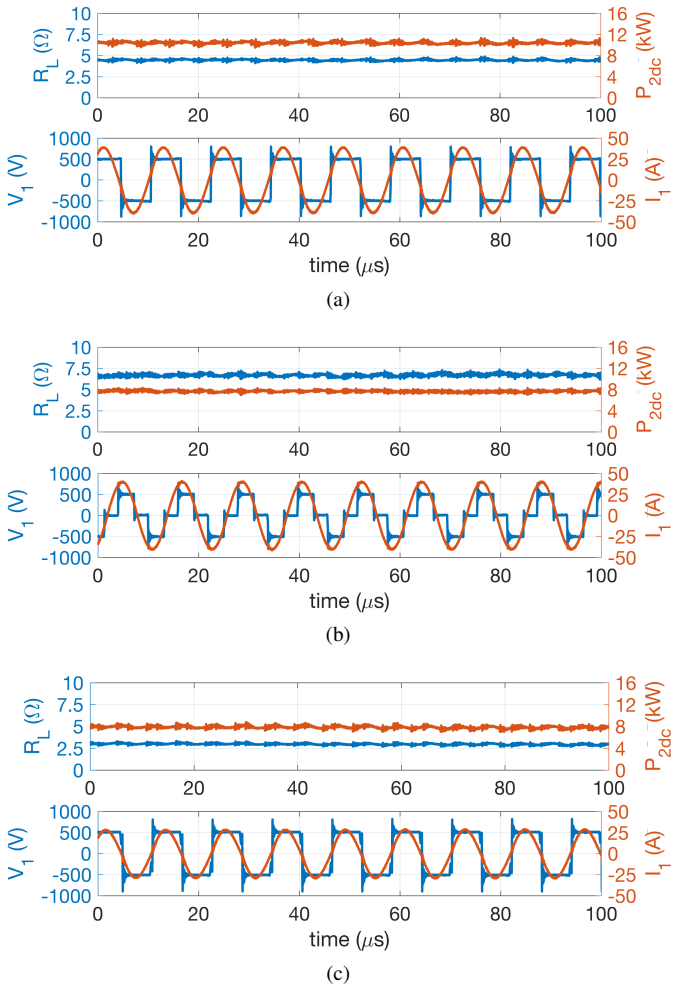

Fig. 14: Waveforms of the dynamic IPT with variation of the demanded power through variation of the equivalent load. (a) refers to the nominal condition with $R_{\mathrm{L}}^{*} = 4.2\ \Omega$ and $P_{2dc} = 11$ kW. (b) refers to a reduced demanded power with $R_{\mathrm{L}}^{*} = 6.6\ \Omega$ and $P_{2dc} = 8$ kW. (c) refers to a reduced demanded power with $R_{\mathrm{L}}^{*} = 3\ \Omega$ and $P_{2dc} = 8$ kW.

current I_1 decreases but the transmitter voltage remains a full square wave. In these conditions the inverter works closer to a zero current commutations with a strong reduction of the commutation losses.

VI. Conclusions

The paper has presented a novel flexible and robust technique for the control of the charging process of a dynamic IPT system based on the control of the equivalent impedance seen on the receiver side. The control of the equivalent load introduces an important benefit represented by the possibility to work with vehicles that have a different power demand by simply varying the value of the controlled load. This change does not influence the behavior of the transmitter side that can continue to operate normally (i.e. independently of load and requested power). The major novel contribution of the present work is the capability offered by the control to manage the overall charging process without requiring any additional sensor for the vehicle identification or any communication link between the two system sides. The flexibility of the system can be enhanced since it is possible to extend the control technique also to other PE architectures under the constraint that a constant load has to be seen by the source. This can be obtained if the control of the receiver side has a faster dynamic response than the control of the transmitter side. As pointed out in the experimental validation, any change in the value of the controlled load introduces a change in the efficiency of the power transfer. The investigation of this effect has been done considering the only part downstream the transmitter converter without considering the effects on the commutation losses. This analysis will be extended in future works. The implemented prototype has shown a good robustness of the control maintaining a stable and continuous power transfer also in presence of strong misalignment guaranteeing the power transfer until a lateral misalignment of 30 cm (with respect to a width of the transmitter of 50 cm). Finally, experimental results have demonstrated a good matching with the theoretical ones, showing that the system can be modeled through a simple circuit model based on the first harmonic approximation. Future improvements will be oriented to the individuation of a proper sequence of a cascade activation of the identification phase in order to reduce the overall system consumption. In a real charging lane constituted by several subsequent transmitters, the activation can be, for instance, controlled through a fast wired communication link in the way that each active coil can lead the subsequent one to the identification phase while other coils can remain in an idle state.

References

[1] U. K. Madawala, M. Neath, and D. J. Thrimawithana, "A Power-Frequency Controller for Bidirectional Inductive Power Transfer Systems," *IEEE Trans. Ind. Electron.*, vol. 60, no. 1, pp. 310–317, Jan. 2013.

[2] J. M. Miller, O. C. Onar, and M. Chinthavali, "Primary-Side Power Flow Control of Wireless Power Transfer for Electric Vehicle Charging," *J. Emerg. Sel. Topics Power Electron.*, vol. 3, no. 1, pp. 147–162, Mar. 2015.

[3] W. Li, H. Zhao, S. Li, J. Deng, T. Kan, and C. C. Mi, "Integrated *LCC* Compensation Topology for Wireless Charger in Electric and Plug-in Electric Vehicles," *IEEE Trans. Ind. Electron.*, vol. 62, no. 7, pp. 4215–4225, Jul. 2015.

[4] *Electric vehicle wireless power transfer (WPT) systems – Part 1: General requirements*, IEC Standard 61980-1:2015.

[5] *Wireless Power Transfer for Light-Duty Plug-In/ Electric Vehicles and Alignment Methodology*, SAE Standard J2954.

[6] M. Yilmaz, V. T. Buyukdegirmenci, and P. T. Krein, "General design requirements and analysis of roadbed inductive power transfer system for dynamic electric vehicle charging," in *2012 IEEE Transportation Electrification Conference and Expo (ITEC)*, pp. 1–6, Jun. 2012.

[7] H. Feng, T. Cai, S. Duan, J. Zhao, X. Zhang, and C. Chen, "An LCC-Compensated Resonant Converter Optimized for Robust Reaction to Large Coupling Variation in Dynamic Wireless Power Transfer," *IEEE Trans. Ind. Electron.*, vol. 63, no. 10, pp. 6591–6601, Oct. 2016.

[8] F. Lu, H. Zhang, H. Hofmann, and C. C. Mi, "A Dynamic Charging System With Reduced Output Power Pulsation for Electric Vehicles," *IEEE Trans. Ind. Electron.*, vol. 63, no. 10, pp. 6580–6590, Oct. 2016.

[9] V. Cirimele, F. Freschi, L. Giaccone, L. Pichon, and M. Repetto, "Human Exposure Assessment in Dynamic Inductive Power Transfer for Automotive Applications," *IEEE Trans. Magn.*, vol. PP, no. 99, pp. 1–1, 2017.

[10] M. Zang, M. Clemens, C. Cimala, J. Streckert, and B. Schmuelling, "Simulation of Inductive Power Transfer Systems Exposing a Human Body with Two-Step Scaled-Frequency FDTD Methods," *IEEE Trans. Magn.*, vol. PP, no. 99, pp. 1–1, 2017.

[11] M. L. G. Kissin, G. A. Covic, and J. T. Boys, "Steady-State Flat-Pickup Loading Effects in Polyphase Inductive Power Transfer Systems," *IEEE Trans. Ind. Electron.*, vol. 58, no. 6, pp. 2274–2282, Jun. 2011.

[12] J. Huh, S. W. Lee, W. Y. Lee, G. H. Cho, and C. T. Rim, "Narrow-Width Inductive Power Transfer System for Online Electrical Vehicles," *IEEE Trans. Power Electron.*, vol. 26, no. 12, pp. 3666–3679, Dec. 2011.

[13] J. Shin, S. Shin, Y. Kim, S. Ahn, S. Lee, G. Jung, S. J. Jeon, and D. H. Cho, "Design and Implementation of Shaped Magnetic-Resonance-Based Wireless Power Transfer System for Roadway-Powered Moving Electric Vehicles," *IEEE Trans. Ind. Electron.*, vol. 61, no. 3, pp. 1179–1192, Mar. 2014.

[14] Q. Zhu, L. Wang, Y. Guo, C. Liao, and F. Li, "Applying LCC Compensation Network to Dynamic Wireless EV Charging System," *IEEE Trans. Ind. Electron.*, vol. 63, no. 10, pp. 6557–6567, Oct. 2016.

[15] C. C. Mi, G. Buja, S. Y. Choi, and C. T. Rim, "Modern Advances in Wireless Power Transfer Systems for Roadway Powered Electric Vehicles," *IEEE Trans. Ind. Electron.*, vol. 63, no. 10, pp. 6533–6545, Oct. 2016.

[16] G. R. Nagendra, L. Chen, G. A. Covic, and J. T. Boys, "Detection of EVs on IPT Highways," *J. Emerg. Sel. Topics Power Electron.*, vol. 2, no. 3, pp. 584–597, Sep. 2014.

[17] C. Park, S. Lee, S. Y. Jeong, G. H. Cho, and C. T. Rim, "Uniform Power I-Type Inductive Power Transfer System With DQ-Power Supply Rails for On-Line Electric Vehicles," *IEEE Trans. Power Electron.*, vol. 30, no. 11, pp. 6446–6455, Nov. 2015.

[18] H. H. Wu, A. Gilchrist, K. D. Sealy, and D. Bronson, "A High Efficiency 5 kW Inductive Charger for EVs Using Dual Side Control," *IEEE Trans. Ind. Informat.*, vol. 8, no. 3, pp. 585–595, Aug. 2012.

[19] T. Diekhans and R. W. D. Doncker, "A Dual-Side Controlled Inductive Power Transfer System Optimized for Large Coupling Factor Variations and Partial Load," *IEEE Trans. Power Electron.*, vol. 30, no. 11, pp. 6320–6328, Nov. 2015.

[20] G. Buja, M. Bertoluzzo, and K. N. Mude, "Design and Experimentation of WPT Charger for Electric City Car," *IEEE Trans. Ind. Electron.*, vol. 62, no. 12, pp. 7436–7447, Dec. 2015.

[21] S. Zhou and C. C. Mi, "Multi-Paralleled LCC Reactive Power Compensation Networks and Their Tuning Method for Electric Vehicle Dynamic Wireless Charging," *IEEE Trans. Ind. Electron.*, vol. 63, no. 10, pp. 6546–6556, Oct. 2016.

[22] B. E. M. S.-A. N. C. Kar, " A Comparative Study of Power Supply Architectures in Wireless EV Charging Systems," *IEEE Trans. Power Electron.*, vol. 30, no. 11, pp. 6408 – 6422, Jun. 2015.

[23] C. Shuwei, L. Chenglin, and W. Lifang, "Research on positioning technique of wireless power transfer system for electric vehicles," in *2014 IEEE Conference and Expo Transportation Electrification Asia-Pacific (ITEC Asia-Pacific)*, pp. 1–4, Aug. 2014.

[24] C.-S. Wang, G. A. Covic, and O. H. Stielau, "Power transfer capability and bifurcation phenomena of loosely coupled inductive power transfer systems," *IEEE Trans. Ind. Electron.*, vol. 51, no. 1, pp. 148–157, Feb. 2004.

[25] V. X. Thai, S. Y. Choi, B. H. Choi, J. H. Kim, and C. T. Rim, "Coreless power supply rails compatible with both stationary and dynamic charging of electric vehicles," in *2015 IEEE 2nd International Future Energy Electronics Conf. (IFEEC)*, pp. 1–5, Nov. 2015.

[26] M. Pahlevaninezhad, P. Das, J. Drobnik, P. K. Jain, and A. Bakhshai, "A ZVS Interleaved Boost AC/DC Converter Used in Plug-in Electric Vehicles," *IEEE Trans. Power Electron.*, vol. 27, no. 8, pp. 3513–3529, Aug. 2012.

[27] B. A. Miwa, D. M. Otten, and M. E. Schlecht, "High efficiency power factor correction using interleaving techniques," in *Appl. Power Electronics Conference and Expo, 1992. APEC '92. Conf. Proc. 1992., Seventh Ann.*, pp. 557–568, Feb. 1992.

[28] V. Cirimele, F. Freschi, and M. Mitolo, "Inductive power transfer for automotive applications: State-of-the-art and future trends," in *Industry Applications Society Annual Meeting, 2016 IEEE*, pp. 1–8. IEEE, 2016.

Riccardo Ruffo (S'17) was born in Asti, Italy, in 1991. He received the B.Sc. and M.Sc. degrees in electrical engineering from Politecnico di Torino, Turin, Italy, in 2013 and 2015, respectively. He is currently working toward the Ph.D degree in electrical engineering at the Department of Energy of the Politecnico di Torino. His research interests include control of inductive power transfer systems for electric vehicles, power electronics, and application of SiC semiconductor devices in industrial AC drives.

Vincenzo Cirimele (M'18) was born in Belvedere Marittimo, Italy, in 1987. He received the M.Sc. degree in electrical engineering at the Politecnico di Torino where he is presently enrolled as Research Fellow at the Department of Energy. From 2015 to 2016 he joined the CNRS laboratory Génie électrique et électronique de Paris (GeePs) in France. On February 2017 he obtained the PhD degree in electronics engineering at the Politecnico di Torino and the PhD degree in electrical engineering at the Université Paris-Saclay. His research interests include protection of people from the magnetic field at industrial frequency, electromagnetic modeling and inductive power transmission for electric vehicles.

Michela Diana received the B.Sc in electrical engineering at the Università degli studi di Cagliari in 2011 and the M.Sc. degree in electrical engineering at the Politecnico di Torino in 2014. Since 2014 she is enrolled as Ph.D. student in Electrical, Electronics and Communication Engineering at the Politecnico di Torino. Her research activities include modeling and design of multi-phase electrical machines and high level control for electric drives and inductive power transfer systems for electric vehicles.

Mojtaba Khalilian was born in Isfahan, Iran. He received the B.Sc. and M.Sc. degrees in electrical engineering from Islamic Azad University, Isfahan, Iran, in 2007 and 2011, respectively. He is currently working toward the Ph.D. degree at Politecnico di Torino, Turin, Italy. His research interests include control of wireless power transfer system, soft-switching techniques in high-frequency DC-DC and DC-AC converters, and resonant power conversion.

Alessandro La Ganga was born in Milazzo, Italy, in 1990. He received the B.Sc. from the Università di Catania, Catania, Italy in 2013 and the M.Sc. in electrical engineering from Politecnico di Torino, Turin, Italy in 2016. He is currently a Ph.D. student at the Politecnico di Torino where he is working in the field of design and control of power converters.

Paolo Guglielmi was born in Imperia, Italy, in 1970. He received the M.Sc. degree in electronic engineering and the PhD degree in electrical engineering from the Politecnico di Torino, Turin Italy, in 1996 and 2001 respectively. Since 2012 he is Associate Professor at the same university at the Department of Energy. His fields of interest are power electronics, high-performance servo drives, and computer-aided design of electrical machines, always in the field of the electric traction. He is active member of IEEE IAS IES and PES international scientific societies and he has authored more than 100 papers published in technical journals and conference proceedings.